Available online at www.sciencedirect.com
ScienceDirect
Solid State Communications 139 (2006) 516–521
solid state communications
www.elsevier.com/locate/ssc

Ab initio P–T phase diagram of $NaBH_4$

Geunsik Lee[a,*], Jin-Yang Lee[b], Jai Sam Kim[a]

[a] *Department of Physics, Pohang University of Science and Technology, Pohang 790-784, Republic of Korea*
[b] *Hynix Semiconductor Inc., San 136-1, Ami-ri, Bubal-eup, Ichon-si Kyoungki-do, 476-701, Republic of Korea*

Received 26 June 2006; accepted 17 July 2006 by J.R. Chelikowsky
Available online 2 August 2006

Abstract

We have studied structural stability of cubic ($Fm\bar{3}m$) and tetragonal ($P\bar{4}2_1c$) phases of $NaBH_4$ in the P–T plane. Electronic density of states and dielectric constants (ϵ_∞), and phonon dispersion curves are also obtained. Well known disordering of $[BH_4]^-$ tetrahedra in the cubic phase is approximated by 2:2 ordering along [110]. The resulting transition temperature (T_c) at 0 is 133 K, which is similar to the experimental value ($T_c = 190$ K). The P–T phase diagram is compared with the recently reported experiment for low pressure range, where our result agrees with the experiment qualitatively.

PACS: 63.20.Dj; 64.70.Kb; 71.15.Mb

Keywords: A. $NaBH_4$; D. Electronic structure; D. Phase diagram

1. Introduction

Alkali borohydrides MBH_4 (M = alkali metal) have attracted considerable attention for hydrogen storage [1], because they have high hydrogen content (up to 18.4 wt% in $LiBH_4$). However there is one problem in practical applications. It requires rather high temperatures to dissociate hydrogen due to strong covalent and ionic bonds. To overcome such limitations, a great deal of research has been conducted focused on catalytic agents. For example Ni_xB catalyst shows greatly enhanced catalytic activity and operational stability in the hydrolysis reaction of $NaBH_4$ [2] which is a promising system for application in fuel cell technology. With the help of a catalyst agent the exothermal reaction, $NaBH_4 + 2H_2O \rightarrow NaBO_2 + 4H_2$, can operate at ambient conditions. Furthermore $NaBO_2$ can be used to regenerate $NaBH_4$ through a fuel recovery reaction.

The structure of the low temperature phase of $LiBH_4$ is orthorhombic with *Pnma* symmetry. Around $T = 384$ K [3] $LiBH_4$ undergoes a structural transformation, but there is controversy about the symmetry of the high temperature phase formed. While an old report [4] claims that it belongs to the tetragonal type, a recent study [5] shows that the symmetry is hexagonal ($P6_3mc$). Recently both proved to be incorrect by ab initio calculation [6], which proposed a new stable phase of *Cc* symmetry. The theoretically found structure was consistent with the experimental X-ray diffraction pattern. Other MBH_4 (M = Na, K, Rb, Cs) compounds show a similar structural phase transition with respect to temperature. At high temperature they crystallize into NaCl-type structures, in which $[BH_4]^-$ is octahedrally surrounded by M^+. H atoms in a $[BH_4]^-$ unit are tetrahedrally oriented about B and along all cube diagonals. This gives a random distribution of $[BH_4]^-$ tetrahedron in two different configurations. At low temperature for M = Na, K, they transform into the same tetragonal phase, in which disordered $[BH_4]$ tetrahedra become ordered along [001] at 190 K for Na [7], and 70 K for K [8,9]. For M = Rb, Cs, they maintain the structure of the high temperature phase, but specific heat anomalies have been observed at 27 K and 44 K respectively [8]. Recently light breaks in the slope of the cell parameters are detected at 22 K and 35 K [9]. These results suggest that there should be some kind of phase transition for M = Rb, Cs.

Even though there are many investigations about the structural transition of the technologically important hydrogen

* Corresponding author. Tel.: +82 54 279 5523; fax: +82 54 279 3099.
E-mail address: maxgeun@physics.postech.ac.kr (G. Lee).

0038-1098/$ - see front matter © 2006 Elsevier Ltd. All rights reserved.
doi:10.1016/j.ssc.2006.07.019

storage material $NaBH_4$, ambiguities still exist especially about the pressure-induced transitions. The analysis of the Raman spectra at room temperature showed the transition at 15 GPa [10], where the high pressure phase is suggested to be either orthorhombic-like or monoclinic-like. Ab initio calculations performed in Ref. [10] showed that cubic $NaBH_4$ ($F\bar{4}3m$) transforms to the monoclinic ($P2_1/c$) at 19 GPa and subsequently to the orthorhombic (*Pnma*) at 33 GPa. However, X-ray diffraction experiments [11] reported transitions of a cubic ($Fm\bar{3}m$) to a tetragonal ($P\bar{4}2_1c$) at 6.3 GPa and further to an orthorhombic (*Pnma*) phase at 8.9 GPa. An experimental P–T phase diagram [12], which was reported this year, showed a cubic–tetragonal transition within a 0–2 GPa range.

In spite of many experimental works, the theoretical P–T phase diagram of $NaBH_4$ has not been reported yet. In this work we report a P–T phase diagram of the technologically important fuel cell material, $NaBH_4$, computed with first-principle method. Computational methods are presented in Sections 2 and 3. Section 3 is devoted to free energy evaluation of the disordered cubic phase. Section 4 contains our results for electronic density of states and dielectric constants (ϵ_∞), Born effective charges, phonon dispersion curves, and P–T phase diagram. Finally Section 5 contains the summary.

2. Calculation methods

The calculations were based on density functional theory (DFT) [13] and density functional perturbation theory (DFPT) [14]. We used Teter's parametrization of the exchange–correlation functional, which is based on Ceperley–Alder's local density approximation (LDA) [15]. The present results have been obtained thanks to the use of the ABINIT code [16,17], that is based on pseudopotentials and planewaves. It relies on an efficient Fast Fourier Transform algorithm [18] for the conversion of wavefunctions between real and reciprocal space, on the adaptation to a fixed potential of the band-by-band conjugate gradient method [19] and on a potential-based conjugate-gradient algorithm for the determination of the self-consistent potential [20]. Technical details on the computation of responses to atomic displacements and homogeneous electric fields can be found in Ref. [21], while Ref. [22] presents the subsequent computation of dynamical matrices, Born effective charges, dielectric permittivity tensors, and interatomic force constants.

Pseudopotentials (PPs) that we used are of the Troullier–Martins [23] type in fully non-local form and obtained from the ABINIT home page. For Na and H, partial core corrections are included. Each 3s, 2s2p, 1s orbital of Na, B, H is treated as valence. Total number of valence electrons per $NaBH_4$ is eight. PPs are tested by computing lattice constants of tetragonal and cubic phases of $NaBH_4$ and comparing with other results. This is given by Table 1. Considering that LDA underestimates lattice constants by 1–3%, our results agree with the experimental values well. For the Brillouin zone sampling we used $8 \times 8 \times 8$ Monkhorst–Pack [24] meshes for both phases. The plane wave kinetic energy cutoff of 47 Ha was used. We confirmed these parameters provide convergence of the total energy to within 0.1 meV/(formula unit), of the pressure to 0.1 GPa, and of the phonon frequency to 2 cm^{-1}. In calculating phonon frequency, we need to find a configuration corresponding to minimum energy to avoid a negative value of frequency. Ions are slightly relaxed until each ion force is less than 10^{-5} Ha/a_0 (a_0: bohr radius).

Table 1
Calculated unit-cell dimensions (in Å), atom coordinates of $NaBH_4$

Space group	Unit-cell dimension	Atom coordinates
$Fm\bar{3}m$	$a = 5.9178$	Na (4*a*): 0, 0, 0
		B (4*b*): 1/2, 1/2, 1/2
		H (32*f*): x, x, x with $x = 0.3805$
	$a = 6.0609$[a]	$x = 0.3779$[a]
	$a = 6.1480$[b]	$x = 0.3901$[b]
$P\bar{4}2_1c$	$a = 4.2165$	Na (2*a*): 3/4, 1/4, 3/4; B (2*b*): 3/4, 1/4, 1/4
	$c = 5.6865$	H (8*g*): 1/4, −0.0113, −0.1268
	$a = 4.3452$[a]	H (8*g*): 1/4, −0.0182, −0.1303[a]
	$c = 5.8597$[a]	
	$a = 4.3320$[b]	H (8*g*): 1/4, −0.0193, −0.1308[b]
	$c = 5.8690$[b]	

[a] Experimental values from Ref. [28].
[b] Experimental values from Ref. [26].

Thermodynamic functions are computed by quasi-harmonic approximation. Helmholtz free energy $F(T)$, as a function of temperature T, is given by: $F(T) = E_{KS} + E_{ph}(T) - T \cdot S(T)$, where E_{KS} is ground state Khon–Sham total energy and $E_{ph}(T)$, $S(T)$ are phonon contributions of vibration energy, entropy. $E_{ph}(T)$ and $S(T)$ are calculated using the formulae

$$E_{ph}(T) = \frac{\hbar}{2}\int_0^{\omega_{\max}} \omega \coth\left(\frac{\hbar\omega}{2k_BT}\right) g(\omega)\mathrm{d}\omega, \tag{1}$$

$$S(T) = k_B \int_0^{\omega_{\max}} \left[\frac{\hbar\omega}{2k_BT}\coth\frac{\hbar\omega}{2k_BT} - \ln\left\{2\sinh\frac{\hbar\omega}{2k_BT}\right\}\right] g(\omega)\mathrm{d}\omega. \tag{2}$$

It requires the phonon density of states (DOS), $g(\omega)$, which is obtained by integrating the number of phonon states in the frequency range $(\omega, \omega + \mathrm{d}\omega)$ on a dense grid of **q** points in the first Brillouin zone. Typical value of this grid should be $48 \times 48 \times 48$ or larger. Dynamical matrices of the grid are interpolated from the dynamical matrices of a coarse grid, each of which consists of two parts, a short-range interatomic force contribution and a long-range electrostatic term. This coarse grid corresponds to the actual number of dynamical matrices to be calculated. We used a $4 \times 4 \times 4$ grid of **q** points for tetragonal phase and $8 \times 8 \times 8$ for cubic.

3. Free energy calculation

At room temperature $NaBH_4$ crystallizes into a cubic (NaCl-type) structure (α-$NaBH_4$), in which each $[BH_4]^-$ anion is surrounded by six Na^+ ions. Its space group is known to be $Fm\bar{3}m$ [25]. H atoms are tetrahedrally oriented about B and along all cube diagonals. This gives a random distribution of

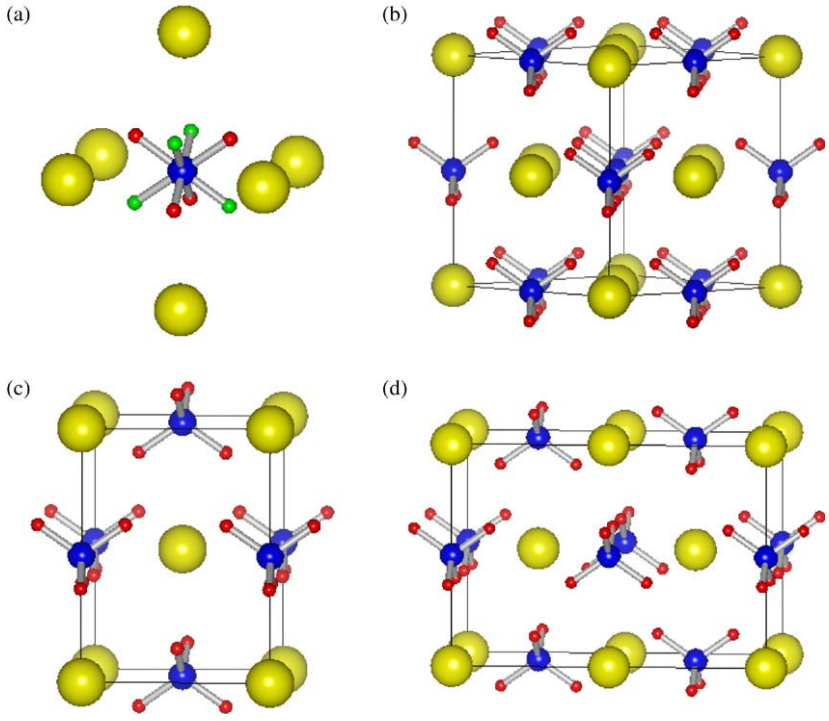

Fig. 1. $NaBH_4$ structures (yellow: Na, blue: B, red and green: H): (a) two different configurations (indicated by red and green colors) of $[BH_4]^-$ in *disFCC* phase ($Fm\bar{3}m$). View along near [1$\bar{1}$0] (cubic reference axis) of (b) *FCC* ($F\bar{4}3m$); only one kind of $[BH_4]^-$, (c) *TET* ($P\bar{4}2_1c$); 1:1 ordering along [101], (d) *FCCsc*; 2:2 ordering along [110]. (For interpretation of the references to colour in this figure legend, the reader is referred to the web version of this article.)

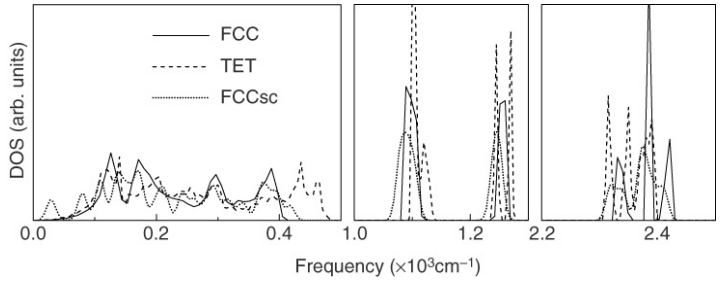

Fig. 2. Phonon DOS of *FCC*, *TET*, and *FCCsc*. Only three energy windows (0–500, 1000–1300, 2200–2500 cm^{-1}) are chosen, because there is no state outside these intervals.

$[BH_4]^-$ tetrahedra in two different configurations which are tridendate and monodendate as shown in Fig. 1(a). We call this kind of phase as *disFCC* which means disordered face-centered cubic (*FCC*). Another type of $[BH_4]^-$ tetrahedra is possible on the *FCC* lattice, the space group of which is $F\bar{4}3m$. The structure is shown in Fig. 1(b). This phase has not been observed experimentally. It is theoretically assumed. We call it *FCC*. At $T = 190$ K α-$NaBH_4$ undergoes a structural transition to β-$NaBH_4$ (tetragonal; $P\bar{4}2_1c$). As shown in Fig. 1(c), where it is denoted by *TET*, there is 1:1 ordering of two $[BH_4]^-$ configurations along [101]. The transition was reported as order–disorder type [26]. As a theoretical model of *disFCC* phase we consider a supercell structure as shown in Fig. 1(d), which has 2:2 ordering along [110]. It is indicated by *FCCsc*.

Free energy is the sum of ground state total energy and phonon contribution. We approximate the phonon contribution of *FCCsc* as the one for *FCC* structure. The approximation is checked by comparison of the phonon density of states (DOS) of *FCC* and *FCCsc*, which is shown in Fig. 2. The phonon DOS of *FCCsc* was calculated as the number of states for a single $\mathbf{q} = (0, 0, 0)$, because the unit cell is so large that one $\mathbf{q}$ point is enough. The phonon DOS of *FCCsc* is very close to that of *FCC* compared to the *TET* case. Actually the phonon contribution is very slight in free energy difference of two phases compared to ground state total energy. As an example of $NaBH_4$, energy differences of *FCC* and *TET* phases are approximately 1 kJ/mol (∼10 meV) for phonon, 100 meV for ground state energy. Therefore it is a valid approximation to replace the phonon DOS of *disFCC* by one of *FCC*. The important quantity is the ground state energy. We compute it accurately for *FCC* and *FCCsc*, which are theoretical models of *disFCC* structure.

To summarize Gibbs free energy of *TET* and *disFCC* as a function of pressure P and temperature T, $G(P, T)$ is expressed as follows

$$G^i(P, T) = E^i_{KS}(V, T = 0) + PV + E^i_{ph}(V) - T \cdot S^i(V), \tag{3}$$

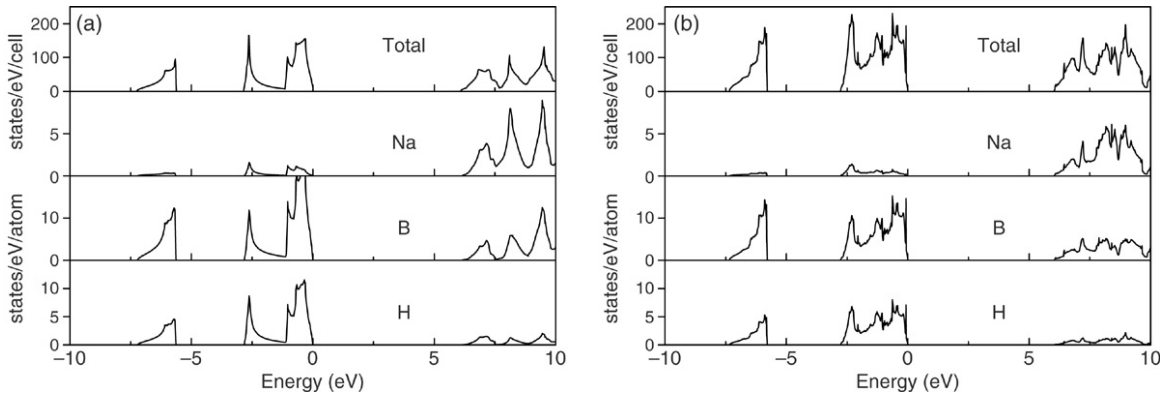

Fig. 3. Total and local DOS projected on each atom for (a) *FCC* and (b) *TET*. Fermi level is set at zero energy. Atomic radius used in projected DOS is 2.0, 1.3, and 1.0 for Na, B, and H in units of bohr radius.

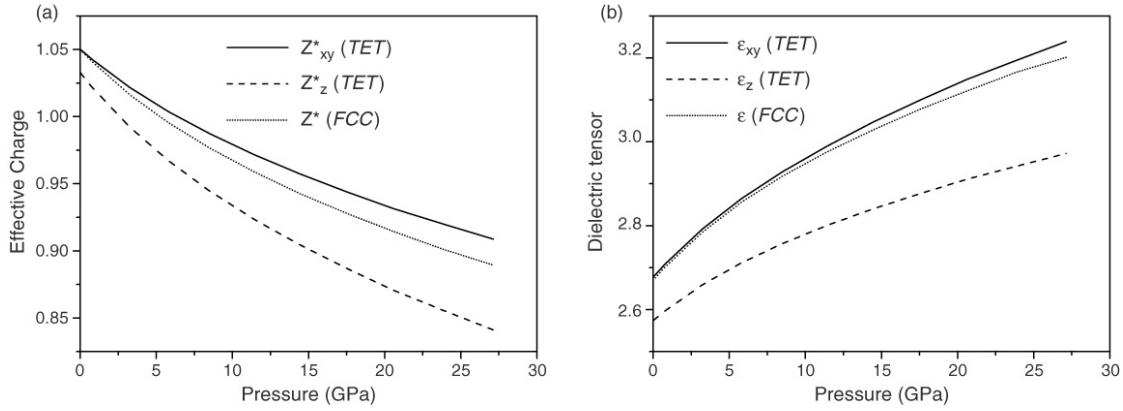

Fig. 4. (a) Born effective charge (Z^*) of Na and (b) high-frequency dielectric constants (ϵ_∞) as a function of pressure. Effective charge of BH_4 is equal to minus the Na charge and B has nearly zero charge.

where i is a phase index ($i = TET$ or $disFCC$) and E^i_{KS} is the ground state Kohn–Sham total energy for a phase i. Pressure P is computed as $P = -\partial E^i_{KS}/\partial V$. E^i_{ph} and S^i are energy and entropy caused by phonons. For $i = TET$ every quantity is given by calculation. For $i = disFCC$ phonon terms are computed from FCC results, the ground state energy is approximated by the energy of FCC or $FCCsc$. The resulting equations are

$$E^{disFCC}_{ph} = E^{FCC}_{ph},$$
$$S^{disFCC} = S^{FCC} + \ln 2,$$
$$E^{disFCC}_{KS} = E^{FCC}_{KS} \quad \text{or} \quad E^{FCCsc}_{KS}. \tag{4}$$

Additional $\ln 2$ in S^{disFCC} is excess entropy due to disorder [27].

4. Results and discussions

In the following we present electronic DOS (4.1), dielectric constants and Born effective charges (4.2), and phonon spectrum (4.3) of *FCC* and *TET* phases. Finally the P–T phase diagram (4.4) is given.

4.1. Electronic DOS

In Fig. 3 total and site-projected DOS of *FCC* and *TET* are shown. There is an energy gap of 6.0 eV between valence and conduction bands, which is similar to 6.5 eV by GGA calculation [28]. The valence band (VB) is split into two bands. The lower band near −6.0 eV is mainly contributed by B-s states and the upper band (−2.0 eV to E_F) by bonding states of B and H. The H-s electrons are tightly bond to the B-p states, and sp^3 hybridization occurs within the BH_4 complex. Contribution by Na in VB is very small, which shows that Na is ionized to Na^+. So $NaBH_4$ has a characteristic of ionic bonding between Na^+ and $[BH_4]^-$. The results of *FCC* and *TET* are roughly the same, but *TET* has more narrow peaks. This is because two BH_4 tetrahedra inside *TET* unit cell have rotational discrepancy of 90° (see Fig. 1(c)), which lowers symmetry.

4.2. Dielectric constants and Born effective charges

Born effective charges (Z^*) and high-frequency dielectric constants (ϵ_∞) of $NaBH_4$ are shown in Fig. 4 for *FCC* and *TET* as a function of pressure. The values of Z^* are +1 for Na, −0.25 for H, and nearly zero for B. From this each Z^* of Na, BH_4 has the value of +1 and −1 respectively. This is consistent with previous electronic DOS analysis. To the best of our knowledge there is no experimental and theoretical data for ϵ_∞. However we can compare indirectly with sodium halides (NaF, NaCl, NaBr, NaI), because bonding characteristics of $NaBH_4$ and sodium halides are very similar. In Table 2 ϵ_∞ of sodium

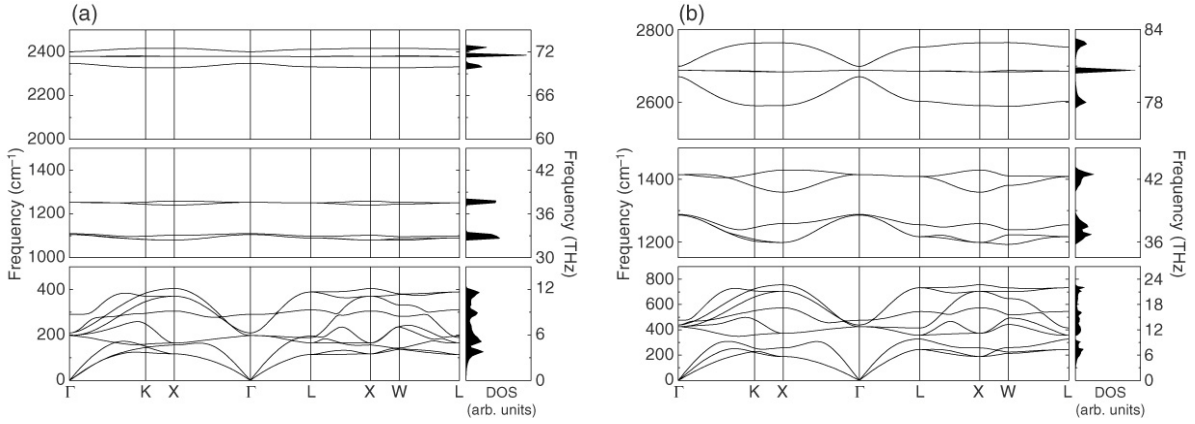

Fig. 5. Phonon band structure and DOS of *FCC* phase at (a) 0 GPa, (b) 27 GPa.

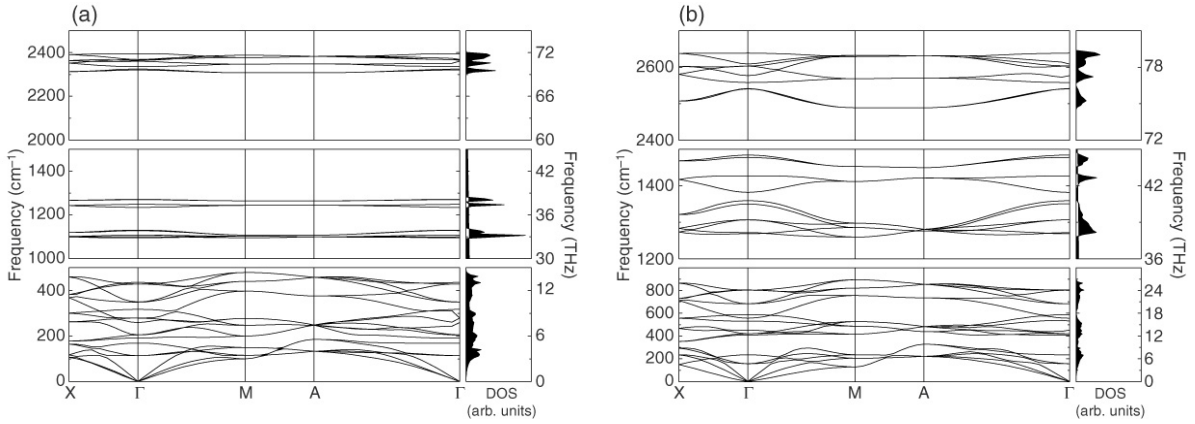

Fig. 6. Phonon band structure and DOS of *TET* phase at (a) 0 GPa, (b) 27 GPa.

Table 2
High-frequency dielectric constants (ϵ_∞) and anion radii of alkali halides

	NaF	NaCl	NaBr	NaI
ϵ_∞[a]	1.74	2.34	2.59	2.93
Anionic radius (Å)[b]	1.19	1.67	1.82	2.06

[a] Ref. [29].
[b] Ref. [30].

halides as well as ionic radii of anions are given. The calculated ϵ_∞ of $NaBH_4$ is 2.68 for $P = 0$ GPa, which is mostly close to the NaBr case. It is known that LDA overestimates ϵ_∞ by 10% [31]. Regarding this error, $\epsilon_\infty = 2.68 - 0.27 = 2.41$. It lies between those of NaCl and NaBr. If we assume that polarizabilities of $[BH_4]$ and halogen elements are similar, ϵ_∞ is mainly dependent on the size of anion. We can guess that the radius of $[BH_4]^-$ is between the radii of Cl^- and Br^-. The actual radius of $[BH_4]$ can be computed as the sum of a B–H distance and a radius of H, which is $2.31a_0+1a_0 = 1.75$ Å. The radius of $[BH_4]^-$ would be a little larger than 1.75 Å, which is close to the Br^- case. It is consistent with the prediction by ϵ_∞. As to comparing lattice constants of NaCl-type crystal structures, the calculated unit cell size of *FCC*-$NaBH_4$ ($a = 5.92$ Å) is very similar to that of NaBr (NaF: 4.62, NaCl: 5.64, NaBr: 5.97, NaI: 6.47). Pressure derivative of ϵ_∞ is to be positive [32], which is consistent with our results.

Table 3
Phonon frequencies (in cm^{-1}) of cubic and tetragonal $NaBH_4$ by our calculation and Raman experiments

ω	Cubic	Tetragonal
ν_1	2385 (2332[a])	2394 (2341[b])
ν_2	1098 (1121[a])	1267 (1280[b])
ν_4	1251 (1277[a])	1120 (1148[b])

[a] Ref. [10].
[b] Ref. [33].

4.3. Phonon spectrum

In Figs. 5 and 6, phonon band structure and DOS of *FCC* and *TET* phases are shown for $P = 0$, 27 GPa. There is no negative frequency, which means all structures are dynamically stable. Raman spectrum of $NaBH_4$ has been studied in Refs. [33] and [10]. Dominant modes were reported to be B–H stretching mode ν_1 and B–H bending modes ν_2, ν_4. As shown in Table 3 our calculated phonon frequencies agree well with Raman experimental results.

4.4. Phase diagram

To get the phase diagram, we have calculated E^i_{KS} ($i = FCC, TET$) for 12 unit cell volumes, which correspond to 12 pressure values ranging from 0 to 27 GPa with compression. For each volume energy $E^i_{ph}(V)$ and entropy $S^i(V)$ of phonons

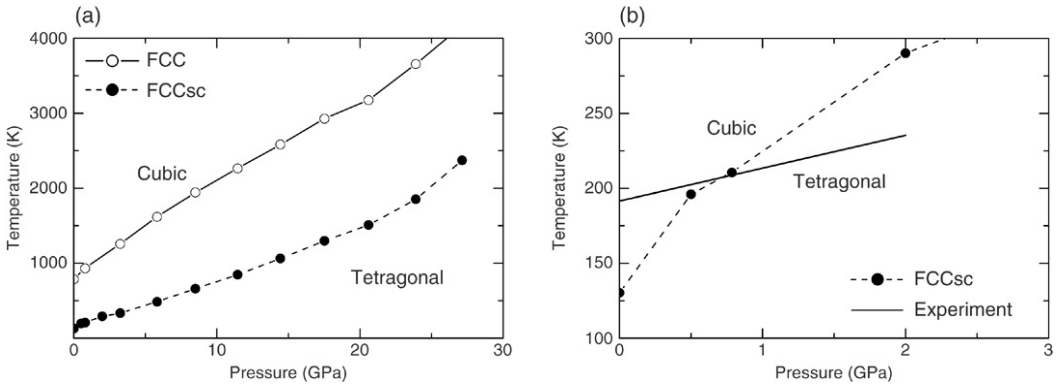

Fig. 7. P–T phase diagram of $NaBH_4$. (a) Phase boundaries are drawn by joining transition points. To obtain the transition points two approximations (*FCC* and *FCCsc*) for *disFCC* are used. (b) Phase boundary for low pressure range together with experimental result of Ref. [12].

were calculated. Then Gibbs free energies as a function of temperature for given 12 pressures are obtained by Eq. (3). The resulting phase diagram is shown in Fig. 7. For all pressures considered here, *disFCC* (*TET*) phase is more stable at high (low) temperature. Transition temperature (T_c) is different depending on the approximation of E_{KS} for *disFCC* (*FCC* or *FCCsc*) as explained in Eq. (4). At $P = 0$ GPa, T_c is 784 K using *FCC* and 133 K using *FCCsc*. T_c of *FCCsc* is lower than that of *FCC*, because E_{KS} per $NaBH_4$ is 45.3 meV lower for *FCCsc*. The experimental value of T_c is 190 K [7]. The discrepancy originates from that we neglect disordering of BH_4 (*FCC*) or consider 2:2 ordering along [110] (*FCCsc*). In Fig. 7(b) we compare with experimental P–T phase diagram [12] (only $0 \leq P \leq 2$ GPa is available). Compression increases the cubic-to-tetragonal transformation temperature. Even at room temperature ($T = 293$ K) the tetragonal phase begins to form at 2.3 GPa in our result and 4.6 GPa in Ref. [12]. In spite of the approximation used, our result qualitatively agrees well with the experiment.

5. Summary

In this paper we have shown the P–T phase diagram of $NaBH_4$ together with electronic density of states and dielectric constants (ϵ_∞), and phonon dispersion curves. Well known disordering of $[BH_4]^-$ tetrahedra in the cubic phase is approximated by 2:2 ordering along [110]. Our calculated temperature of cubic–tetragonal transition at 0 GPa is 133 K, which agrees reasonably with the experimental value ($T_c = 190$ K). Also the phase diagram qualitatively agrees well with the recently reported experiment for low pressure range. Phonon frequencies are in good accordance with results of Raman experiments. Calculated ϵ_∞ is 2.68, which is shown to be quite reasonable.

Acknowledgements

This work was supported by Postech BSRI Research Fund 2006. The authors would like to acknowledge the support from KISTI (Korea Institute of Science and Technology Information) under [The 7th Strategic Supercomputing Support Program] with Dr S.M. Lee as the technical supporter. The use of the computing system of the Supercomputing Center is also greatly appreciated.

References

[1] Z.P. Li, B.H. Liu, N. Morigasaki, S. Suda, J. Alloys Compd. 354 (2003) 243 (and references therein).
[2] D. Hua, Y. Hanxi, A. Xinping, C. Chuansin, Int. J. Hydrogen Energ. 28 (2003) 1095.
[3] S. Gomes, H. Hagemann, K. Yvon, J. Alloys Compd. 346 (2002) 206.
[4] C.W.F.T. Pistorius, Z. Phys. Chem. Neue Fol. 88 (1974) 253; K.N. Semenko, A.P. Chavgun, V.N. Surov, Russian J. Inorg. Chem. 16 (1971) 271.
[5] J-Ph. Soulié, G. Renaudin, R. Černý, K. Yvon, J. Alloys Compd. 346 (2002) 200.
[6] Z. Łodziana, T. Vegge, Phys. Rev. Lett. 93 (2004) 145501.
[7] H.L. Johnston, N.C. Hallett, J. Amer. Chem. Soc. 75 (1953) 1467.
[8] C.C. Stephenson, D.W. Rice, W.H. Stockmayer, J. Chem. Phys. 23 (1955) 1960.
[9] G. Renaudin, S. Gomes, H. Hagemann, L. Keller, K. Yvon, J. Alloys Compd. 375 (2004) 98.
[10] C.M. Araújo, R. Ahuja, A.V. Talyzin, B. Sundqvist, Phys. Rev. B 72 (2005) 054125.
[11] R.S. Kumar, A.L. Cornelius, Appl. Phys. Lett. 87 (2005) 261916.
[12] B. Sundqvist, O. Andersson, Phys. Rev. B 73 (2006) 092102.
[13] P. Hohenberg, W. Kohn, Phys. Rev. 136 (1964) B864; W. Kohn, L.J. Sham, Phys. Rev. 140 (1965) A1133.
[14] S. Baroni, P. Giannozzi, A. Testa, Phys. Rev. Lett. 58 (1987) 1861.
[15] D.M. Ceperley, B.J. Alder, Phys. Rev. Lett. 45 (1981) 566.
[16] X. Gonze et al., Comput. Mater. Sci. 25 (2002) 478.
[17] The ABINIT code is a common project of the Université Catholique de Louvain, Corning Incorporated, and other contributors (URL: http://www.abinit.org).
[18] S. Goedecker, SIAM J. Sci. Comput. 18 (1997) 1605.
[19] M.C. Payne, M.P. Teter, D.C. Allan, T.A. Arias, J.D. Joannopoulos, Rev. Mod. Phys. 64 (1992) 1045.
[20] X. Gonze, Phys. Rev. B 54 (1996) 4383.
[21] X. Gonze, Phys. Rev. B 55 (1997) 10337.
[22] X. Gonze, C. Lee, Phys. Rev. B 55 (1997) 10355.
[23] N. Troullier, J.L. Martins, Phys. Rev. B 43 (1991) 1993.
[24] H.J. Monkhorst, J.D. Pack, Phys. Rev. B 13 (1976) 5188.
[25] R.L. Davis, C.H.L. Kennard, J. Solid State Chem. 59 (1985) 393.
[26] P. Fischer, A. Zuttel, Mater. Sci. Forum 443–444 (2004) 287.
[27] W.H. Stockmayer, C.C. Stephenson, J. Chem. Phys. 21 (1953) 1311.
[28] P. Vajeeston, P. Ravindran, A. Kjekshus, H. Fjellvåg, J. Alloys Compd. 387 (2005) 97.
[29] N.W. Ashcroft, N.D. Mermin, Solid State Physics, Saunders College, Orlando, 1976, p. 553.
[30] R.D. Shannon, Acta Crystallogr. A 32 (1976) 751.
[31] X. Gonze, Ph. Ghosez, R.W. Godby, Phys. Rev. Lett. 74 (1995) 4035.
[32] L.K. Banerjee, A.N. Basu, S. Sengupta, Phys. Rev. B 20 (1979) 1706.
[33] K.B. Harvey, N.R. McQuaker, Canad. J. Chem. 49 (1971) 3282.